INORGANIC CHEMISTRY
FRONTIERS

RESEARCH ARTICLE

View Article Online
View Journal | View Issue

Cite this: *Inorg. Chem. Front.*, 2023, **10**, 3860

Halogenation triggering rules in hybrid materials for fluorescence and dielectric phase transitions†

Jun-Qin Wang, Gele Teri, Hao-Fei Ni, Qing-Feng Luo, Xiao-Ping Wang, Da-Wei Fu, * Yi Zhang * and Qiang Guo *

Received 30th March 2023,
Accepted 21st May 2023

DOI: 10.1039/d3qi00594a

rsc.li/frontiers-inorganic

Organic–inorganic hybrid materials with controllable physicochemical properties have played a great role in multifunctional sensors, photovoltaic cells, switching devices, *etc*. Among them, organic–inorganic hybrid dielectric materials have become a hot research topic within current cross-frontier research. In order to unveil the effect of halogen ions on phase transitions, we synthesized three hybrids: (TMBPA)$CdCl_2Br$ (TMBPA-ClBr, **1**), $(TMBPA)_2CdBr_4$ (TMBPA-Br, **2**), and $(TMIPA)_2CdI_4$ (TMIPA-I, **3**), (TMBPA = 3-bromopropyltrimethylammonium, TMIPA = 3-iodopropyltrimethylammonium). The phase-transition temperature of the three compounds increases with the size of the halogen ions from Cl^- to I^-. Interestingly, the three compounds exhibit consistent trends in dielectric and photoluminescence properties, and the corresponding photoluminescence lifetimes are calculated as 1.55 ns, 1.28 ns, and 0.98 ns, expressing consistency with halogen regulation. This is very similar to the success of the cationic substitution of formamidinium/Cs/methylammonium lead iodide. Therefore, this work provides guidance for understanding the composition–structure–property relationship of organic–inorganic hybrid perovskites.

Introduction

The intersection and integration of disciplines is the current thinking in terms of a way to break through the shackles of the disciplines and explore scientific challenges. For example, the process from material preparation to device implementation and device upgrading, which reversely promotes materials optimization, needs to be solved in an interdisciplinary way.[1–7] The exploration of molecular-based phase-transition materials and devices is one method used in the development and progress of such characteristics. Therefore, multiple methods, such as the development of spherical-like and non-spherical structures, physical symmetry breaking, and chemical synthesis, are combined together.[8–15] Among them, the chemical synthesis method of some important materials includes metal-ion replacement and doping, which deduces the regulation of the non-metal; that is, the exploration of the role of halogens in materials synthesis.[16–21] This work focuses on this halogenation rule, and there are few reports on the regulation rule. The organic–inorganic hybrid compounds were chosen due to their facile structural design and tunability. This will be described in detail and summarized in this study.

Organic–inorganic hybrid materials with excellent photoelectric properties have shown great potential for various applications, as mentioned above. The hybrids possess merits of mechanical flexibility, feasibility of film processing, low production-energy consumption, and highly tunable structures and properties, and they have received a lot of attention from researchers.[22–26] A series of new organic–inorganic hybrid materials with excellent properties have emerged one after another under the full cooperation and joint efforts of research teams at home and abroad.[27,28] The polar structures and phase transitions of these compounds mostly result from the adjustment of molecular size, structure and intermolecular interactions, such as hydrogen bonding,[29–32] coordination or halogen–halogen bonds, which lead to symmetry breaking at low temperatures and the formation of low-symmetry polar structures, thus triggering phase transitions.[33–36]

Since 2009, organic–inorganic hybrid materials have gradually emerged and attracted worldwide research interest. In 2016, Ye *et al.* successfully achieved the modulation of ferroelectricity and the narrow band gap of halide perovskites through halogen doping, which opened up a broad application prospect for halide perovskites in the field of semiconducting ferroelectrics.[37] In 2019, Xiong' s team creatively proposed the "Quasi-Spherical" and "momentum matching" theories to successfully realize the design of molecular ferroelectrics.[38] In

Institute for Science and Applications of Molecular Ferroelectrics, Key Laboratory of the Ministry of Education for Advanced Catalysis Materials, Zhejiang Normal University, Jinhua, 321004, China. E-mail: dawei@zjnu.edu.cn

†Electronic supplementary information (ESI) available: PXRD, variable-temperature powder X-ray diffraction, ultraviolet-vis absorption spectra and detailed structural data. CCDC 2220969–2220975. For ESI and crystallographic data in CIF or other electronic format see DOI: https://doi.org/10.1039/d3qi00594a

2021, Luo *et al.* demonstrated lead-free halide perovskite heterogeneous crystals and provided significant insights into the assembly of various sustainable and miniaturized perovskite optoelectronic devices.[39] These representative works point out the direction for the research of organic–inorganic hybrid perovskites. However, the understanding of the composition–structure–property relationship of organic–inorganic hybrid perovskites is not yet deep, and additional research is required to explore this aspect further.

Inspired by previous works, we introduced a 3-bromopropyl group into trimethylammonium, and successfully synthesized (TMBPA)$CdCl_2Br$ (TMBPA-ClBr, **1**) $(TMBPA)_2CdBr_4$ (TMBPA-Br, **2**), and $(TMIPA)_2CdI_4$ (TMIPA-I, **3**), (TMBPA = 3-bromopropyltrimethylammonium, TMIPA = 3-iodopropyltrimethylammonium). We found that as the size of the halogen ion increases, the phase-change temperature increases. Furthermore, the three compounds all have fluorescent properties. These findings add more members to the family of organic–inorganic hybrid perovskites, and also provide a guide to understanding the composition–structure–property relationship of organic–inorganic hybrid perovskites.

Experimental section

Syntheses of (TMBPA)$CdCl_2Br$, $(TMBPA)_2CdBr_4$ and $(TMIPA)_2CdI_4$

3-Bromopropyltrimethylammonium bromide (2 mmol, 0.52 g), and $CdCl_2$ (2 mmol, 0.37 g), were added to a mixture of hydrochloric acid (10 mL) and ethanol (10 mL), and the above solution was stirred. Colorless, transparent crystals were obtained after 3–4 days at room temperature. The crystallization method of $(TMBPA)_2CdBr_4$ and $(TMIPA)_2CdI_4$ was the same as that of (TMBPA)$CdCl_2Br$, only replacing $CdCl_2$ with $CdBr_2$ (2 mmol, 0.69 g) or CdI_2 (2 mmol, 0.73 g), respectively.

Single-crystal X-ray diffraction

Using a Bruker APEX-II CCD diffractometer, the diffraction data before and after the phase-transition temperature of the three compounds were measured and collected separately with a Mo source. Data processing was performed using APEX3. In the SHELXLTL package, the crystal structure was directly solved and refined by the f^2-based full-matrix least-squares method. All non-hydrogen atoms were anisotropically refined using all reflections of $I > 2\sigma(I)$ and hydrogen atoms were geometrically positioned in appropriate locations. In addition, calculations involving angles and distances between some atoms were measured by DIAMOND and SHELXLTL. Other relevant crystallographic data for each of the three compounds are listed in the ESI.†

Dielectric properties and DSC measurements

Dielectric measurements. The dried compound was pressed into flakes by a tablet press. The flakes were then cut to the appropriate size, fixed to the capacitor with carbon or silver paste, and then the temperature-dependent permittivity of heating and cooling was measured using a Tonghui TH2828A instrument in a frequency range of 5 kHz to 1 MHz. Differential scanning calorimetry (DSC) measurements were performed using a NETZSCH-214 instrument. 10 mg or so of sample powders was weighed into an aluminum crucible and then heated and cooled in a nitrogen atmosphere at a rate of 20 K per minute.

Ultraviolet–visible (UV-vis) spectroscopy

UV-near-infrared-visible (UV-NIR-vis) spectra were obtained on a Cary RF 6000 instrument, and the fluorescence spectra were measured on an FLS 9801 instrument.

Results and discussion

As can be seen from Scheme 1, the three compounds are synthesized from the same starting organic ammonium salt, but have different structures and compositions. To make it easier to distinguish, the atoms after the disorder has occurred are shown in a different color from the original ones, *e.g.*, the disordered atoms of C are shown in black. The order–disorder change of organic cations induces the occurrence of a phase transition in the three compounds.

Crystal structure and intermolecular interaction analysis

Single-crystal X-ray diffraction analysis was performed at the pre- and post-phase-transition temperatures. For convenience, the phase below the phase-transition temperature is labelled as the low-temperature phase (LTP), the phase between the two phase temperatures as the intermediate-temperature phase (ITP), and the phase above the phase-transition temperature as the high-temperature phase (HTP). Powder X-ray diffraction

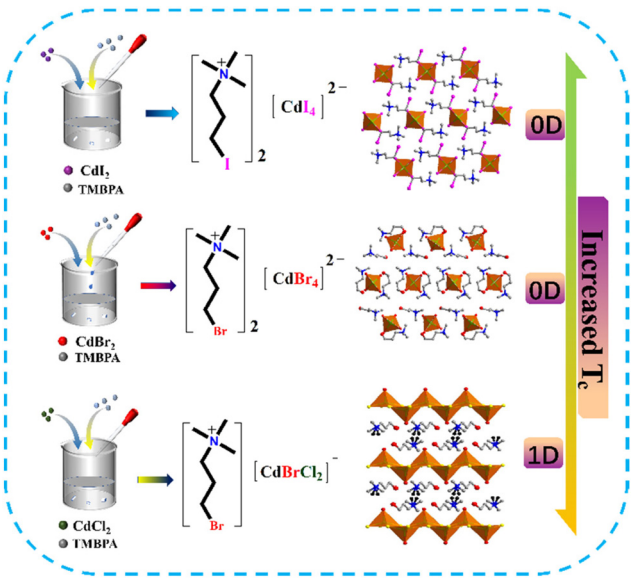

Scheme 1 Diagram of the detailed design route through halogen regulation.

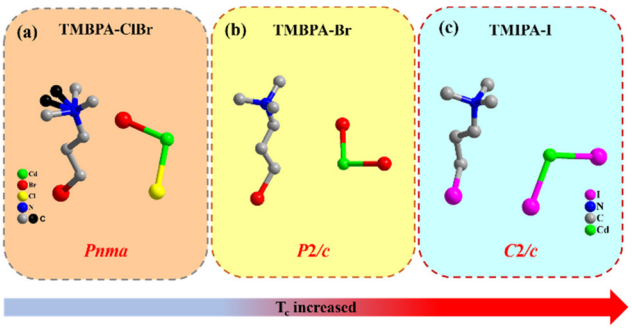

Fig. 1 The asymmetric units of (a) TMBPA-ClBr, (b) TMBPA-Br, and (c) TMIPA-I in the LTP (all hydrogen atoms were omitted for clarity).

(PXRD) results of the three compounds are found to be consistent with the simulated PXRD spectra, demonstrating their high phase purity (Fig. S1†). The asymmetric units of TMBPA-ClBr, TMBPA-Br, and TMIPA-I in the LTP are displayed in Fig. 1.

In the LTP, TMBPA-ClBr crystallizes in the *Pnma* space group of the orthorhombic crystal system with cell parameters of a = 11.635(3) Å, b = 7.3428(14) Å, c = 15.379(4) Å, and V = 1314.0(5) Å^3 (Table S1†). The inorganic part of TMBPA-ClBr exhibits a distinct one-dimensional chain structure in the LTP, (Fig. 2a) where Cd forms a five-coordinate configuration with Cl and Br. When the temperature increases to 385.15 K, the crystal crystallizes in the *Cmcm* space group, which belongs to the orthogonal crystal system. The cell parameters are a = 15.411(14) Å, b = 11.677(9) Å, c = 7.365(7) Å, and V = 1325(2) Å^3 (Table S1†). At high temperature, its cell parameters are a = 15.479(5) Å, b = 11.741(3) Å, c = 7.402(2) Å, and V = 1345.2(7) Å^3 (Table S1†). The crystal structure is shown in Fig. 2c. By comparison, the cell parameters of TMBPA-ClBr in the ITP and the HTP do not change much. However, the crystal structure in the HTP shows that the cations become more disordered, so this compound undergoes an isomorphic phase transition from medium to high temperatures. Phase transition usually causes distortion of the inorganic skeleton, as shown in Fig. 2d–f, which shows the bond angle change of the inorganic skeleton of the TMBPA-ClBr from low to high temperature. As the temperature increases, the bond angle between the Br and Cl atoms changes from 107.02(28)° to 106.23(34)° to 106.22(8)°. There are some corresponding changes in the bond angles between the other atoms as well. This suggests that the slight distortion of the inorganic skeleton is also related to the phase transition.

For TMBPA-Br and TMIPA-I, we focus on the description of TMBPA-Br because these two compounds have a similar phase-transition behavior. The crystal structures of TMIPA-I are shown in Fig. S2† and crystallographic data and structural refinement details are shown in Table S3.† As can be seen from the unit-cell diagram in Fig. 3a, TMBPA-Br at low temperature crystallizes in the *P*2/*c* space group of the monoclinic crystal system with cell parameters of a = 24.015(7) Å, b = 9.642(3) Å, c = 16.046(4) Å, β = 91.474(5)° and V = 3714.4(18) Å^3 (Table S2†). Upon increasing the temperature to 381.5 K, the cation goes from an ordered to a disordered state (Fig. 3d). In the ITP, the space group changes to *C*2/*c* in the monoclinic crystal system with cell parameters of a = 33.148(18) Å, b = 9.669(6) Å, c = 15.960(8) Å, β = 96.244(9)° and V = 5085(5) Å^3 (Table S2†). Unfortunately, we could not obtain the high-temperature structure of TMBPA-Br, but we performed variable-temperature PXRD characterization of this compound (Fig. S3†). With the increase of temperature, we can see a very obvious change in the diffraction peaks of this compound before and after the phase transition, which confirms that TMBPA-Br undergoes two reversible phase transitions. The organic amine cations of TMBPA-Br in the low- and intermediate-temperature structures are shown in Fig. 3b and e. It can be seen that the organic amine cations undergo a transformation during the order to disorder phenomenon upon an increase in temperature, similar to skiers going from single-board to double-board skiing behavior. In addition to this, the distance between adjacent cadmium atoms was also analyzed, as shown in Fig. 3c and f. The distance between adjacent cadmium atoms became smaller from low to medium temp-

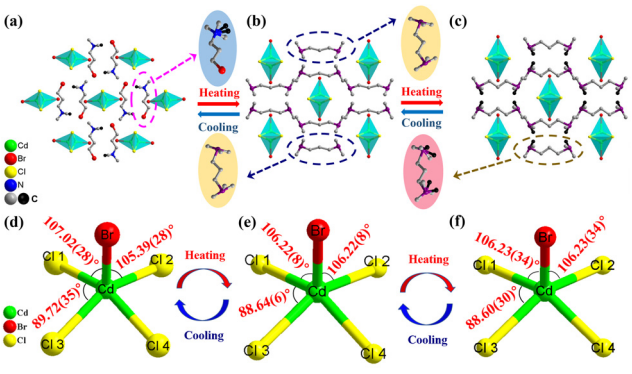

Fig. 2 (a) The crystal structures (without hydrogen atoms) of TMBPA-ClBr in the LTP, (b) ITP and (c) HTP. (d) The inorganic skeleton-key angles of TMBPA-Br in the LTP, (e) ITP and (f) HTP.

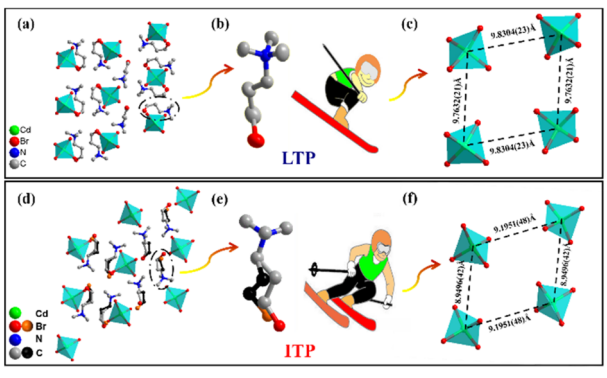

Fig. 3 (a) Packing structure of TMBPA-Br in the LTP and (d) the ITP (hydrogen atoms are omitted). (b) The organic ammonium cation of TMBPA-Br in the LTP and (e) the ITP. (c) The adjacent metal-distance skeleton of TMBPA-Br in the LTP and (f) the ITP.

erature, which may be caused by the disorder of organic amines from low to medium temperature.

We further calculated and evaluated Hirshfeld surfaces and two-dimensional (2D) fingerprints to better understand how intermolecular interactions affect the properties of the compounds. For clear analysis and comparison, the focus will be on selected cations that have relatively strong contacts in each structure. The organic ammonium portion shown in Fig. 4 has a dark red surface, indicating a strong interaction between the organic and inorganic portions of TMBPA-ClBr. By comparing the hydrogen-bonding forces of the three compounds, TMBPA-ClBr, TMBPA-Br and TMIPA-I, it can be seen from Fig. 4 that the hydrogen-bonding forces increase sequentially from 19.9% to 36.7% to 37.0%, thus indicating that the structures of the three compounds change with the regulation of halogens, and indirectly proving that the phase-transition temperature of the three compounds increases sequentially as the halogen atom becomes larger.

Thermal analysis

Differential scanning calorimetry (DSC) is a thermal analysis method that can effectively represent the relationship between the individual phases of a substance as a function of temperature and is therefore an effective method for characterizing phase transitions.[40–43]

The DSC plots of the compounds TMBPA-ClBr, TMBPA-Br and TMIPA-I are presented in Fig. 5a. It can be seen that TMBPA-ClBr at 369 K/349.9 K and 397.8 K/386.9 K (heating/cooling) shows two pairs of reversible endothermic/exothermic peaks, which indicates that TMBPA-ClBr undergoes two temperature-induced reversible phase transitions. Similarly, two pairs of reversible endothermic/exothermic peaks at 381.5 K/354.7 K and 414.9 K/404.1 K are also observed for TMBPA-Br, revealing that TMBPA-Br possesses two reversible phase transitions. Unlike the first two compounds, TMIPA-I has a pair of reversible peaks at 424.8 K/397.4 K as seen in the DSC plot, suggesting that TMIPA-I has a reversible phase transition. The

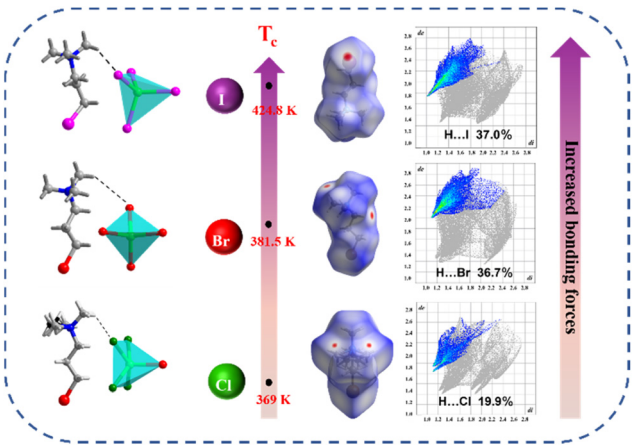

Fig. 4 Hirshfeld d_{norm} surfaces and fingerprint plots for TMBPA-ClBr, TMBPA-Br, and TMIPA-I.

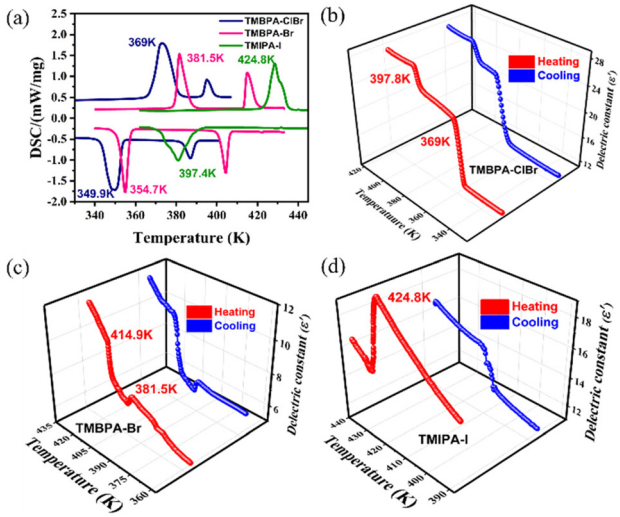

Fig. 5 (a) DSC curves of TMBPA-ClBr, TMBPA-Br, and TMIPA-I recorded on heating. Dielectric constant *vs.* temperature for (b) TMBPA-ClBr, (c) TMBPA-Br, and (d) TMIPA-I recorded at 1 MHz.

DSC cooling plots of the three compounds are shown in Fig. S4.†

From the above DSC and dielectric analyses, it can be confirmed that the three compounds have indeed undergone phase transitions. The phase transition temperature (T_c) seen from the DSC plots has changed due to the modulation of halogens. By further analysis of the DSC diagrams, the entropy changes of TMBPA-ClBr, TMBPA-Br, and TMIPA-I are about 34.81 J mol^{-1} K^{-1}, 61.34 J mol^{-1} K^{-1} and 59.33 J mol^{-1} K^{-1}, respectively. The values of N derived from the Boltzmann equation ($\Delta S = R \ln(N)$, where R is the gas constant and N is the ratio of possible logarithms) are 66.68, 1603 and 1261.4.

The dielectric constant is one of the most important parameters characterizing the physical properties of compounds.[44–47] The dielectric constant can be obtained at different temperatures and can elucidate certain rules of the material structure and the mechanisms of polarization, relaxation and resonance of each microstructural component within the material, as well as the mutual rules between them. Dielectric measurements were carried out on the powder samples of compounds **1–3** using a dielectric meter, and the dielectric plots of the three compounds are shown in Fig. 5b, c and d, respectively. Taking Fig. 5b as an example, it can be seen that two pairs of obvious step-like anomalies appear for TMBPA-ClBr as the temperature changes, indicating dual phase transitions. The abrupt change of dielectric constant (ε') near the phase-transition temperature is consistent with the DSC results. Likewise, the dielectric plots of TMBPA-Br, and TMIPA-I are also in agreement with the DSC results. Multi-frequency dielectric curves are shown in Fig. S4.†

Optical properties

Photoluminescent materials can be applied to light-emitting diodes (LEDs), which have the advantages of being energy-

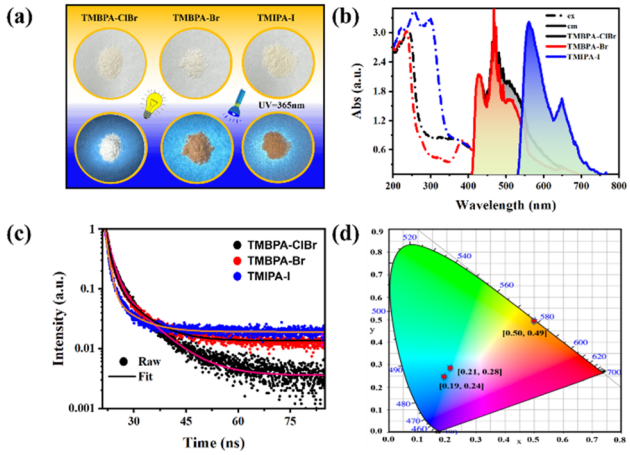

Fig. 6 (a) Photographs of the three compounds under natural light and UV irradiation at 365 nm. (b) Excitation and emission spectra of the three compounds. (c) The fluorescence lifetimes of the three compounds. (d) CIE chromaticity coordinates of the three compounds.

efficient, environmentally friendly, fully solid-state and long-lasting, and are one of the important ways for human beings to solve the energy crisis in the 21st century.[48–52] As shown in Fig. 6a, the three compounds appear white under natural light, and exhibit stable white, orange and deep-orange colors under 365 nm UV light, respectively. The maximum excitation and emission wavelengths of the three compounds were recorded using a 420 nm filter. As shown in Fig. 6b, the UV spectra of the three compounds consist of UV absorption peaks at 384 nm, 384 nm and 372 nm, and the fluorescence spectra show high emission peaks at 467 nm, 468 nm and 648 nm. The fluorescence lifetimes of the three compounds are calculated to be 1.55 ns, 1.28 ns and 0.98 ns (Fig. 6c), respectively. To quantitatively describe the colors of the three compounds, a chromaticity coordinate diagram is presented (Fig. 6d). To evaluate the suitability of the compounds for photovoltaics, for example, as shown in Fig. S5,† band gaps (E_g) of the compounds TMBPA-ClBr, TMBPA-Br, and TMIPA-I were estimated to be about 3.361 eV, 4.306 eV, and 4.498 eV, respectively, by calculating the Tauc plots[53,54] (inset of Fig. S5†), which indicates that TMBPA-ClBr has the potential to become a potential application for semiconductors.

Conclusions

In summary, we have successfully synthesized three organic–inorganic hybrid compounds by a halogen substitution strategy, two of which undergo dual phase transitions, while the third shows a single phase transition. The phase-transition mechanism of the three compounds is attributed to the order–disorder change of organic cations, and the phase-transition temperature is controlled by the halogen modulation effect, which successfully reflects the regulation of halogenation. The increase of phase-transition temperature from compound **1** to compound **3** is caused by the enhanced hydrogen-bonding force. In addition, all three compounds exhibit excellent photoluminescence properties. In conclusion, this work plays a very positive role in promoting the regulation of dielectric, ferroelectric and optical materials, to enrich interdisciplinary research methods, and provide a broad prospect for the design of organic–inorganic hybrid multifunctional optoelectronic materials.

Conflicts of interest

There are no conflicts to declare.

Acknowledgements

This work was financially supported by the Natural Science Foundation of Zhejiang Province (LZ20B010001).

References

1 Z. X. Zhang, C. Y. Su, J. Li, X. J. Song, D. W. Fu and Y. Zhang, Ferroelastic Hybrid Bismuth Bromides with Dual Dielectric Switches, *Chem. Mater.*, 2021, **33**, 5790–5799.
2 A. Sultana, P. Sadhukhan, M. M. Alam, S. Das, T. R. Middya and D. Mandal, Organo-Lead Halide Perovskite Induced Electroactive beta-Phase in Porous PVDF Films: An Excellent Material for Photoactive Piezoelectric Energy Harvester and Photodetector, *ACS Appl. Mater. Interfaces*, 2018, **10**, 4121–4130.
3 X. J. Song, Z. X. Zhang, X. G. Chen, H. Y. Zhang, Q. Pan, J. Yao, Y. M. You and R. G. Xiong, Bistable State of Protons for Low-Voltage Memories, *J. Am. Chem. Soc.*, 2020, **142**, 9000–9006.
4 D. W. Fu, W. Zhang, H. L. Cai, Y. Zhang, J. Z. Ge, R. G. Xiong and S. D. Huang, Supramolecular bola-like ferroelectric: 4-methoxyanilinium tetrafluoroborate-18-crown-6, *J. Am. Chem. Soc.*, 2011, **133**, 12780–12786.
5 T. Zhang, K. Xu, J. Li, L. He, D. W. Fu, Q. Ye and R. G. Xiong, Ferroelectric hybrid organic-inorganic perovskites and their structural and functional diversity, *Natl. Sci. Rev.*, 2023, **10**, nwac240.
6 L. P. Miao, N. Ding, N. Wang, C. Shi, H. Y. Ye, L. Li, Y. F. Yao, S. Dong and Y. Zhang, Direct observation of geometric and sliding ferroelectricity in an amphidynamic crystal, *Nat. Mater.*, 2022, **21**, 1158–1164.
7 M. Ma Czka, A. Nowok, J. K. Zareba, D. Stefanska, A. Ga Gor, M. Trzebiatowska and A. Sieradzki, Near-Infrared Phosphorescent Hybrid Organic-Inorganic Perovskite with High-Contrast Dielectric and Third-Order Nonlinear Optical Switching Functionalities, *ACS Appl. Mater. Interfaces*, 2022, **14**, 1460–1471.
8 J. Harada, Plastic/ferroelectric molecular crystals: Ferroelectric performance in bulk polycrystalline forms, *APL Mater.*, 2021, **9**, 020901.

9 X. J. Song, T. Zhang, Z. X. Gu, Z. X. Zhang, D. W. Fu, X. G. Chen, H. Y. Zhang and R. G. Xiong, Record Enhancement of Curie Temperature in Host-Guest Inclusion Ferroelectrics, *J. Am. Chem. Soc.*, 2021, **143**, 5091–5098.

10 Y. Yao, Y. Peng, L. Li, X. Zhang, X. Liu, M. Hong and J. Luo, Exploring a Fatigue-Free Layered Hybrid Perovskite Ferroelectric for Photovoltaic Non-Volatile Memories, *Angew. Chem., Int. Ed.*, 2021, **60**, 10598–10602.

11 X. Zheng, P.-P. Shi, Y. Lu, L. Zhou, J.-X. Gao, F.-J. Geng, D.-H. Wu, D.-W. Fu and Q. Ye, Dielectric and nonlinear optical dual switching in an organic–inorganic hybrid relaxor $[(CH_3)_3PCH_2OH][Cd(SCN)_3]$, *Inorg. Chem. Front.*, 2017, **4**, 1445–1450.

12 Y. Zhao, P. Zhu, S. Huang, S. Tan, M. Wang, R. Wang, J. Xue, T. H. Han, S. J. Lee, A. Zhang, T. Huang, P. Cheng, D. Meng, J. W. Lee, J. Marian, J. Zhu and Y. Yang, Molecular Interaction Regulates the Performance and Longevity of Defect Passivation for Metal Halide Perovskite Solar Cells, *J. Am. Chem. Soc.*, 2020, **142**, 20071–20079.

13 D. W. Fu, J. X. Gao, P. Z. Huang, R. Y. Ren, T. Shao, L. J. Han, J. Liu and J. M. Gong, Observation of Transition from Ferroelasticity to Ferroelectricity by Solvent Selective Effect in Anilinium Bromide, *Angew. Chem., Int. Ed.*, 2021, **60**, 8198–8202.

14 K. Li, Z. G. Li, J. Xu, Y. Qin, W. Li, A. Stroppa, K. T. Butler, C. J. Howard, M. T. Dove, A. K. Cheetham and X. H. Bu, Origin of Ferroelectricity in Two Prototypical Hybrid Organic-Inorganic Perovskites, *J. Am. Chem. Soc.*, 2022, **144**, 816–823.

15 W. J. Xu, K. Romanyuk, J. M. G. Martinho, Y. Zeng, X. W. Zhang, A. Ushakov, V. Shur, W. X. Zhang, X. M. Chen, A. Kholkin and J. Rocha, Photoresponsive Organic-Inorganic Hybrid Ferroelectric Designed at the Molecular Level, *J. Am. Chem. Soc.*, 2020, **142**, 16990–16998.

16 W. Q. Liao, Y. Y. Tang, P. F. Li, Y. M. You and R. G. Xiong, Competitive Halogen Bond in the Molecular Ferroelectric with Large Piezoelectric Response, *J. Am. Chem. Soc.*, 2018, **140**, 3975–3980.

17 N. Zhang, Y. Zhang, H.-H. Jiang, G.-W. Du, Q. Pan, R.-G. Xiong and H.-Y. Zhang, Enantiomeric Hydrogen-bonded Chains Driving Ferroelectric and Nonlinear Optical Behavior, *Chem. Mater.*, 2022, **34**, 8077–8086.

18 H. F. Ni, L. K. Ye, P. C. Zhuge, B. L. Hu, J. R. Lou, C. Y. Su, Z. X. Zhang, L. Y. Xie, D. W. Fu and Y. Zhang, A nickel(II)-based one-dimensional organic-inorganic halide perovskite ferroelectric with the highest Curie temperature, *Chem. Sci.*, 2023, **14**, 1781–1786.

19 D. W. Fu, J. X. Gao, W. H. He, X. Q. Huang, Y. H. Liu and Y. Ai, High-T(c) Enantiomeric Ferroelectrics Based on Homochiral Dabco-derivatives (Dabco = 1,4-Diazabicyclo[2.2.2]octane), *Angew. Chem., Int. Ed.*, 2020, **59**, 17477–17481.

20 Y. Xue, Z. Zhang, P.-P. Shi, W. Zhang, Q. Ye and D. Fu, High-temperature dielectric switch and second harmonic generation integrated in a stimulus responsive material, *Chin. Chem. Lett.*, 2021, **32**, 539–542.

21 Y.-Z. Wang, P.-P. Shi, K. Xu, L. He, X. Meng and Q. Ye, Dielectric switching, SHG response and Pd(ii) adsorption of a multifunctional phase-transition complex, *Inorg. Chem. Front.*, 2021, **8**, 4858–4863.

22 C. F. Wang, H. Li, Q. Ji, C. Ma, L. Liu, H. Y. Ye, B. Cao, G. Yuan, H. F. Lu, D. W. Fu, M. G. Ju, J. Wang, K. Zhao and Y. Zhang, Discovery of a 2D Hybrid Silver/Antimony–Based Iodide Double Perovskite Photoferroelectric with Photostrictive Effect and Efficient X–Ray Response, *Adv. Funct. Mater.*, 2022, **32**, 2205918.

23 D. X. Liu, H. L. Zhu, W. X. Zhang and X. M. Chen, Nonlinear Optical Glass-Ceramic From a New Polar Phase-Transition Organic-Inorganic Hybrid Crystal, *Angew. Chem., Int. Ed.*, 2023, **62**, e202218902.

24 Z. B. Hu, C. F. Wang, T. T. Sha, C. Shi, L. Ye, H. Y. Ye, Y. Song, Y. M. You and Y. Zhang, An Effective Strategy of Introducing Chirality to Achieve Multifunctionality in Rare-Earth Double Perovskite Ferroelectrics, *Small Methods*, 2022, **6**, e2200421.

25 A. Zeb, Z. Sun, T. Khan, M. A. Asghar, Z. Wu, L. Li, C. Ji and J. Luo, [C5H12N]CdCl3: an ABX3 perovskite-type semiconducting switchable dielectric phase transition material, *Inorg. Chem. Front.*, 2017, **4**, 1485–1492.

26 M. Rok, B. Zarychta, R. Janicki, M. Witwicki, A. Bienko and G. Bator, Dielectric-OpticalSwitches: Photoluminescent, EPR, and Magnetic Studies on Organic-Inorganic Hybrid $(azetidinium)_2MnBr_4$, *Inorg. Chem.*, 2022, **61**, 5626–5636.

27 T. Zhang, C. Chen, W.-Y. Zhang, Q. Ye and D.-W. Fu, Heat-sensitive structural phase transitions of hybrid halide perovskite with double dielectric ON/OFF switches, *Inorg. Chem. Front.*, 2018, **5**, 2340–2345.

28 Y. Yu, P. Huang, Y. Wang, Z. Zhang, T. Zhang, Y. Zhang and D. Fu, X-site doping in ABX3 triggers phase transition and higher Tc of the dielectric switch in perovskite, *Chin. Chem. Lett.*, 2021, **32**, 3558–3561.

29 H. Xu, W. Guo, Y. Ma, Y. Liu, X. Hu, L. Hua, S. Han, X. Liu, J. Luo and Z. Sun, Record high-Tc and large practical utilization level of electric polarization in metal-free molecular antiferroelectric solid solutions, *Nat. Commun.*, 2022, **13**, 5329.

30 Z.-X. Zhang, T. Zhang, P.-P. Shi, W.-Y. Zhang, Q. Ye and D.-W. Fu, Exploring high-performance integration in a plastic crystal/film with switching and semiconducting behavior, *Inorg. Chem. Front.*, 2020, **7**, 1239–1249.

31 Y. Wang, T. Zhang, M.-M. Lun, F.-L. Zhou, D.-W. Fu and Y. Zhang, Halogen regulation triggers NLO and dielectric dual switches in hybrid compounds with green fluorescence, *Inorg. Chem. Front.*, 2021, **8**, 4230–4238.

32 W. J. Xu, P. F. Li, Y. Y. Tang, W. X. Zhang, R. G. Xiong and X. M. Chen, A Molecular Perovskite with Switchable Coordination Bonds for High-Temperature Multiaxial Ferroelectrics, *J. Am. Chem. Soc.*, 2017, **139**, 6369–6375.

33 J. X. Gao, W. Y. Zhang, Z. G. Wu, Y. X. Zheng and D. W. Fu, Enantiomorphic Perovskite Ferroelectrics with Circularly Polarized Luminescence, *J. Am. Chem. Soc.*, 2020, **142**, 4756–4761.

34 T. Zhang, J.-Y. Li, G.-W. Du, K. Ding, X.-G. Chen, Y. Zhang and D.-W. Fu, Thermally-driven unusual dual SHG switching with wide SHG-active steps triggered by inverse symmetry breaking, *Inorg. Chem. Front.*, 2022, **9**, 4341–4349.
35 Y. Ai, H.-P. Lv, Z.-X. Wang, W.-Q. Liao and R.-G. Xiong, H/F substitution for advanced molecular ferroelectrics, *Trends Chem.*, 2021, **3**, 1088–1099.
36 X. G. Chen, X. J. Song, Z. X. Zhang, P. F. Li, J. Z. Ge, Y. Y. Tang, J. X. Gao, W. Y. Zhang, D. W. Fu, Y. M. You and R. G. Xiong, Two-Dimensional Layered Perovskite Ferroelectric with Giant Piezoelectric Voltage Coefficient, *J. Am. Chem. Soc.*, 2020, **142**, 1077–1082.
37 H. Y. Ye, W. Q. Liao, C. L. Hu, Y. Zhang, Y. M. You, J. G. Mao, P. F. Li and R. G. Xiong, Bandgap Engineering of Lead-Halide Perovskite-Type Ferroelectrics., *Adv. Mater.*, 2016, **28**, 2579–2586.
38 H. Y. Zhang, Y. Y. Tang, P. P. Shi and R. G. Xiong, Toward the Targeted Design of Molecular Ferroelectrics: Modifying Molecular Symmetries and Homochirality, *Acc. Chem. Res.*, 2019, **52**, 1928–1938.
39 X. Zhang, T. Zhu, C. Ji, Y. Yao and J. Luo, In Situ Epitaxial Growth of Centimeter-Sized Lead-Free (BA) 2CsAgBiBr7/Cs2AgBiBr6 Heterocrystals for Self-Driven X-ray Detection, *J. Am. Chem. Soc.*, 2021, **143**, 20802–20810.
40 Z. S. Yao, K. Yamamoto, H. L. Cai, K. Takahashi and O. Sato, Above Room Temperature Organic Ferroelectrics: Diprotonated 1,4-Diazabicyclo[2.2.2]octane Shifts between Two 2-Chlorobenzoates, *J. Am. Chem. Soc.*, 2016, **138**, 12005–12008.
41 M.-M. Lun, T. Zhang, C.-Y. Su, J. Li, Z.-X. Zhang, D.-W. Fu and H.-F. Lu, A ferroelastic molecular rotator [$(Me_2N(CH_2)_2NH_3)$(18-crown-6)]triflate with dual dielectric switches, *Mater. Chem. Front.*, 2022, **6**, 1929–1937.
42 H. Y. Zhang, H. H. Jiang, Y. Zhang, N. Zhang and R. G. Xiong, Ferroelectric Lithography in Single-Component Organic Enantiomorphic Ferroelectrics, *Angew. Chem., Int. Ed.*, 2022, **61**, e202200135.
43 L. Xu, X. Mu, X.-G. Chen, H.-Y. Zhang and R.-G. Xiong, Organic Enantiomeric Ferroelectrics with High Piezoelectric Performance: Imidazolium L- and D-Camphorsulfonate, *Chem. Mater.*, 2021, **33**, 5769–5779.
44 Y. Ai, R. Sun, Y. L. Zeng, J. C. Liu, Y. Y. Tang, B. W. Wang, Z. M. Wang, S. Gao and R. G. Xiong, Coexistence of magnetic and electric orderings in a divalent Cr^{2+}-based multiaxial molecular ferroelectric, *Chem. Sci.*, 2021, **12**, 9742–9747.
45 Q. Jia, T. Shao, L. Tong, C. Su, D. Fu and H. Lu, Lead-free bilayer heterometallic halide perovskite with reversible phase transition and photoluminescence properties, *Chin. Chem. Lett.*, 2023, **34**, 107539.
46 J. C. Liu, W. Q. Liao, P. F. Li, Y. Y. Tang, X. G. Chen, X. J. Song, H. Y. Zhang, Y. Zhang, Y. M. You and R. G. Xiong, A Molecular Thermochromic Ferroelectric, *Angew. Chem., Int. Ed.*, 2020, **59**, 3495–3499.
47 C. Su, Z. Zhang, J. Yao, M. Chen, P. Huang, Y. Zhang, D. Fu and L. Xie, Construction, photoelectric response and phase transition for new hybrid double perovskites showing narrow band gaps, *Chin. Chem. Lett.*, 2023, **34**, 107442.
48 H. Peng, Q. Liu, Y. Liu, Y. Lu and W. Liao, A chiral lead-free tin(IV)-based halide organic-inorganic semiconductor with dielectric switching and phase transition, *Chin. Chem. Lett.*, 2022, 107980.
49 Q. Guo, W.-Y. Zhang, Q. Ye and D.-W. Fu, The First Molecule-Based Blue-Light Optical-Dielectric Switching Material in Both Hybrid Bulk Crystal and Flexible Thin Film Forms, *Adv. Opt. Mater.*, 2017, **5**, 1700743.
50 P.-Z. Huang, H.-F. Ni, C.-Y. Su, M.-M. Lun, H.-F. Lu, D.-W. Fu and Q. Guo, Thermal-Induced Ferroelastics in Two Lead-Free Organic–Inorganic Hybrid Perovskites, *CCS Chem.*, 2022, DOI: **10.31635/ccschem.022.202202332**.
51 J. Y. Li, T. Zhang, M.-M. Lun, Y. Zhang, L. Z. Chen and D. W. Fu, Facile Control of Ferroelectricity Driven by Ingenious Interaction Engineering, *Small*, 2023, e2301364.
52 D. Fu, Z. Hou, Y. He, J.-C. Liu, H.-P. Lv and Y.-Y. Tang, Multiaxial Ferroelectricity and Ferroelasticity in a Chiral Perovskite, *Chem. Mater.*, 2022, **34**, 3518–3524.
53 J. Tauc, R. Grigorovici and A. Vancu, Optical Properties and Electronic Structure of Amorphous Germanium, *Phys. Status Solidi B*, 1966, **15**, 627.
54 R. Suhrmann, M. Kruel and G. Wedler, Elektrischer Widerstand und Elektronen-Austrittspotentiale reiner im Ultrahochvakuum aufgedampfter Germaniumfilme, *Z. Phys.*, 1963, **173**, 71–77.